Finite-element model of the human head: scalp potentials due to dipole sources

Y. Yan[1] P. L. Nunez[2] R. T. Hart[2]

[1]School of Medicine, The George Washington University, Washington, DC 20052, USA
[2]Department of Biomedical Engineering, Tulane University, New Orleans, LA 70018, USA

Abstract—*Three-dimensional finite-element models provide a method to study the relationship between human scalp potentials and neural current sources inside the brain. A new formulation of dipole-like current sources is developed here. Finite-element analyses based on this formulation are carried out for both a three-concentric-spheres model and a human-head model. Differences in calculated scalp potentials between these two models are studied in the context of the forward and inverse problems in EEG. The effects of the eye orbit structure on surface potential distribution are also studied.*

Keywords—*Concentric sphere model, Dipole, EEG, Eye orbit, Finite-element model, Forward solution, Grid density, Internal current field*

Med. & Biol. Eng. & Comput., 1991, **29**, 475–481

1 Introduction

THE PRINCIPAL goal of electroencephalography (EEG) is to relate measured scalp potentials to current sources generated in brain tissue. In some applications, e.g. focal epilepsy, localisation of sources is desired. More generally, one wishes to obtain estimates of the statistical properties of the neural source field from scalp potential data (NUNEZ, 1981). The classical inverse problem in EEG has no unique solution, i.e. any surface potential distribution may be due to many different combinations of brain sources. Thus, all applications involve some version of the constrained inverse problem. Such constraints may require, for example, that sources comprise a small number of dipoles which do not change location over a specified time interval (SCHERG and VON CRAMON, 1985; NUNEZ, 1989; 1990). Alternately, equivalent sources can be constrained to the cortex (NUNEZ, 1981; 1987*a*).

There are many unresolved questions concerning the appropriate choices of constraints in specific EEG applications. This issue is not, however, directly addressed here. Rather, we are concerned here only with the forward problem in which scalp potentials due to known sources are calculated. The accuracy of these forward solutions is, of course, of critical importance to the future development of inverse solutions, in which both constraints and head model determine the applicability and accuracy of the results. For example, random errors with certain RMS values might be added to measured scalp potentials and inverse solutions applied. If these RMS values are of the correct magnitude (as determined by finite-element models), an idea of the expected accuracy of inverse solutions may be obtained.

First received 13th March and in final form 20th September 1990

A number of mathematical models have been used to estimate scalp potentials due to known sources. The most widely used model consists of three concentric spherical surfaces representing brain, skull and scalp tissue (NUNEZ, 1981; PLONSEY, 1969; RUSH and DRISCOLL, 1969). This model has been checked experimentally in a saline-filled skull (RUSH and DRISCOLL, 1968) and has been shown to yield good semi-quantitative agreement with a variety of general observations of EEG (NUNEZ, 1981; 1990). The three-spheres model is, of course, a gross over-simplification of both the geometric and electrical properties of real heads. Thus, it is of interest to consider a more exact numerical solution which accounts for some of the geometric complexities in order to gain some understanding of the magnitudes of errors inherent in the three-sphere model, as, for example, in other numerical approaches (MEIJS and PETERS, 1987). The finite-element model outlined here also omits many important features of real heads; however, it is expected that better methods will be developed in the near future using MRI scans to obtain geometric information, as well as new methods to estimate tissue conductivities (NUNEZ, 1987*b*).

Finite-element methods have been proven to be very effective for solving partial differential equations with complicated solution domain and boundary conditions (Fig. 1). Thus, they can be used to formulate and solve electric field distribution problems for EEG studies (COOK, 1981; HUEBNER and THORNTON, 1984, SEPULVEDA *et al.*, 1983). The application of the finite-element methods to brain modelling problems depends critically on computer technology. A large amount of virtual storage and computing time is required for three-dimensional finite-element models that give satisfactorily detailed descriptions of complicated structures such as a human head. As a result some earlier finite-element models were two-dimensional

versions consisting of either a section or a surface of the head. In these models, the requirement for virtual storage and computing time is much smaller (HE *et al.*, 1987; SEPULVEDA, 1984). However, two-dimensional models are not adequate to describe volume-conduction effects of the conductive medium with sufficient accuracy to be of use in EEG.

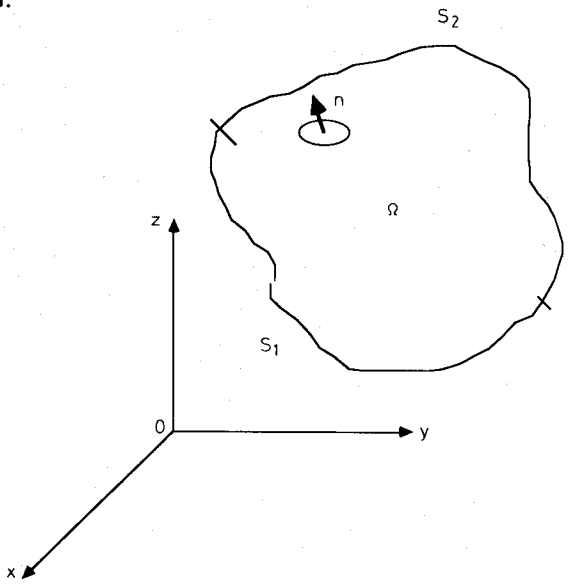

Fig. 1 *Three-dimensional domain Ω in a rectangular co-ordinate system. S_1 and S_2 comprise a close surface of Ω*

In the present study, a new formulation to model dipole current sources is developed; the resulting three-dimensional finite-element code is based on this formulation. In finite-element analyses, a dipole source is usually treated as two point sources which are placed on two nodes of the element(s) during construction of the model (HUEBNER and THORNTON, 1984, SEPULVEDA, 1984), as indicated in Fig. 2. Two disadvantages of this approach are:

(i) Because the pole separation of a 'dipole' is, by definition, very small, at least one edge of an element must be small enough to reflect the dipole size. This may result in a finite-element model consisting of either an unnecessarily large number of elements or elements of inadequate aspect ratio.

(ii) The finite-element model must be altered for different dipole directions. When several dipoles are present, construction and modification of the finite-element model becomes a cumbersome task.

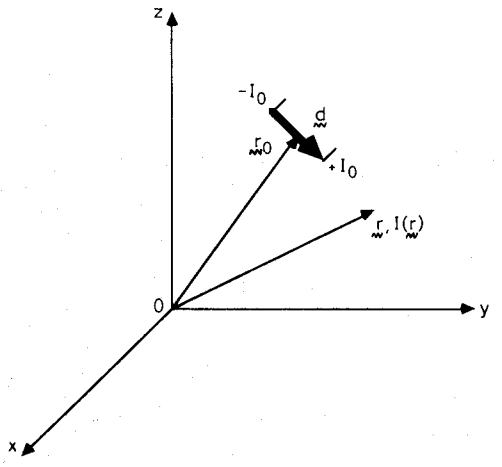

Fig. 2 *Dipole in a three-dimensional space. r_0 is the location of the dipole centre. $+I_0$ and $-I_0$ are the point current source and sink. **d** is the dipole vector from the sink to the source. The resulting current field at a point **r** is given by I(r)*

The new formulation used here treats the dipole as an internal current field. It is shown that this formulation can avoid the two problems listed above. In the results presented here, a finite-element analysis of a three-concentric-spheres model is first carried out. This preliminary study serves to test the validity and accuracy of the new formulation. The three-sphere model also serves the purpose of finding the adequate grid density to be used in the more realistic head studies. A finite-element model based on the geometry of a real human skull, with the scalp and brain tissue simulated, is then constructed and analysed. A comparison is made between the results of the finite-element analyses and results predicted by a three-concentric-spheres model, whose size is obtained by fitting surface points of the scalp to a spherical surface (MEIJS and PETERS, 1987). A further study concerns the effects on scalp potential of the eye orbit region. As irregularity in the geometry of the orbit region makes a local spherical fit especially inadequate, this effect is of special interest in EEG applications.

2 Computer simulations

A three-dimensional finite-element analysis program was developed based on the algorithm described in the Appendix. The 20-noded hexahedral element was used so that the curved geometry of the head could be precisely described and a fast convergence rate achieved. Eqn. 8 of the Appendix was then solved by a wavefront method (HINTON and OWEN, 1984). In some situations, the problem to be analysed is symmetric, so that the finite-element model may include only a part of the symmetric domain; however, the new partial model must preserve the original boundary conditions. In EEG applications, an obvious boundary condition is that no current flows into the air, i.e. $\partial v/\partial \boldsymbol{n} = 0$, where $\boldsymbol{n}$ is the outward normal unit vector of the outer boundary surface. If a half-head model is used, the midline symmetric plane becomes a boundary surface of the finite-element model. To make the midline surface satisfy the above boundary condition (at least approximately), source placement must be restricted. If the current sources are placed in the full head model and oriented symmetrically with respect to the midline plane, no current will flow across this plane, and the original boundary condition is exactly preserved. Alternatively, if the source placement is nonsymmetric, but if these sources are placed far away from the midline plane, current flow across this plane may be sufficiently small to be neglected. The midline boundary condition is then considered approximately satisfied (YAN 1988).

A finite-element model of the three concentric spheres model was first constructed. The purposes of this step were:

(*a*) to verify the correctness of the dipole source formulation developed in the Appendix

(*b*) to find a suitable grid density at which satisfactory accuracy is achieved so that this grid density can be used in later analyses of real heads.

Because of the geometric symmetry of the concentric spheres, our finite-element model only includes half of the spherical surface. The inner, middle, and outer radii of the three spheres are 8·0, 8·5 and 9·0 cm (NUNEZ, 1981), respectively. The conductivity ratio between either scalp or brain tissue and the skull is taken as 80 (RUSH and DRISCOLL, 1968; 1969). A radial dipole is placed in the symmetric plane at a radius of 7·8 cm, corresponding roughly to a neocortical source. A total of 6402 nodes and 1484 elements are included in the model. The results of the

analysis are presented in Fig. 3. Nodal voltages on the outer surface are compared with the analytical values of potential calculated from eqn. 15 of the Appendix. The relative errors at different angles are given in Table 1. This comparison indicates that except for regions very close to the dipole, in which the error is somewhat larger, this grid density yields reasonably accurate results, i.e. errors of the order of 1 per cent.

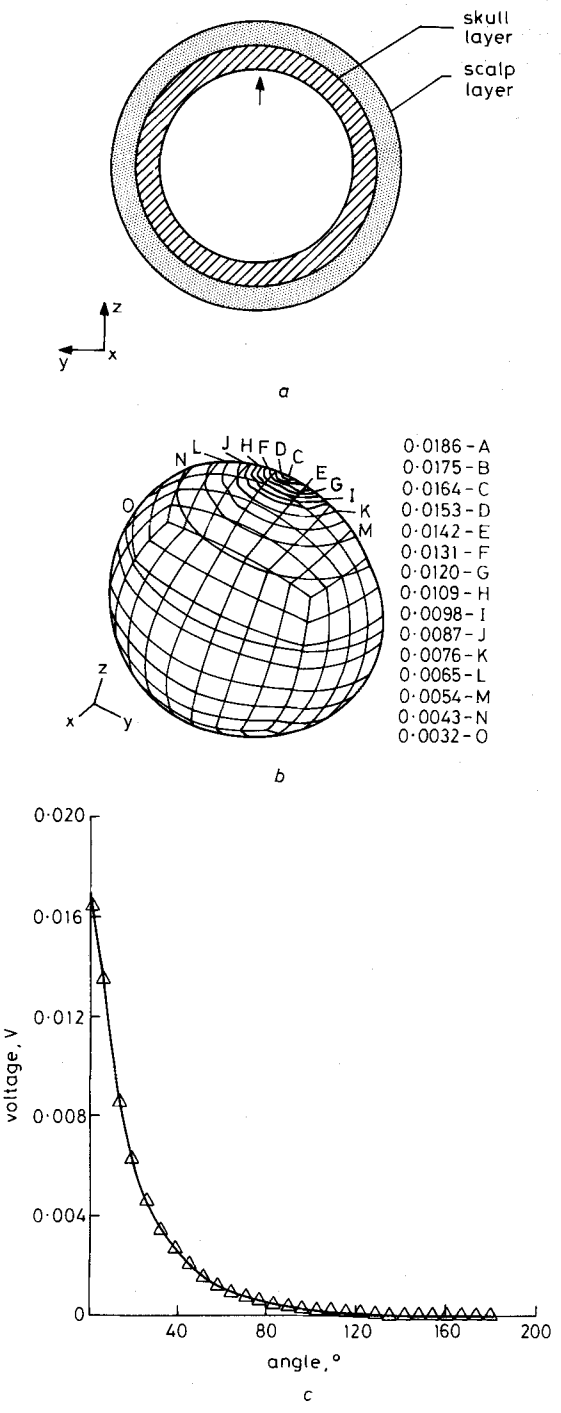

Fig. 3 *Three-dimensional finite-element model consisting of three concentric spherical surfaces and the results of the finite-element analysis. (a) Diagram of the mid-sagittal section of the model. The arrow indicates the location and orientation of the dipole used in the analysis. (b) Finite-element model with isopotential lines of the calculated electric potential. Letters labelled near the contour lines represent potential levels listed in the column on the right. (c) Comparison between the results of the finite-element analysis and the analytic solution for the three-concentric-sphere model as a function of angle from the dipole, measured along the mid-sagittal direction*

——— *analytical values* △ *finite-element values*

Table 1 Comparison between finite-element analysis results and analytical solutions of a three-concentric-sphere model at different angles

Angle, °	Analytical, V	Finite-element, V	Error, per cent
0·0	$1·724 \times 10^{-2}$	$1·642 \times 10^{-2}$	−4·7
6·4	$1·326 \times 10^{-2}$	$1·345 \times 10^{-2}$	1·5
12·9	$0·863 \times 10^{-2}$	$0·857 \times 10^{-2}$	−0·7
19·3	$0·621 \times 10^{-2}$	$0·625 \times 10^{-2}$	0·6
25·7	$0·456 \times 10^{-2}$	$0·458 \times 10^{-2}$	0·4
32·1	$0·343 \times 10^{-2}$	$0·342 \times 10^{-2}$	−0·3
38·6	$0·264 \times 10^{-2}$	$0·264 \times 10^{-2}$	0·2
45·0	$0·203 \times 10^{-2}$	$0·204 \times 10^{-2}$	0·1
51·4	$0·158 \times 10^{-2}$	$0·158 \times 10^{-2}$	−0·1
57·9	$0·125 \times 10^{-2}$	$0·125 \times 10^{-2}$	0·0
64·3	$0·098 \times 10^{-2}$	$0·098 \times 10^{-2}$	0·0
70·7	$0·078 \times 10^{-2}$	$0·078 \times 10^{-2}$	0·0
77·1	$0·062 \times 10^{-2}$	$0·062 \times 10^{-2}$	0·0
83·6	$0·049 \times 10^{-2}$	$0·049 \times 10^{-2}$	0·0
90·0	$0·041 \times 10^{-2}$	$0·041 \times 10^{-2}$	0·5
96·4	$0·031 \times 10^{-2}$	$0·031 \times 10^{-2}$	0·3
102·8	$0·024 \times 10^{-2}$	$0·024 \times 10^{-2}$	−0·1
109·3	$0·019 \times 10^{-2}$	$0·019 \times 10^{-2}$	0·1
115·7	$0·014 \times 10^{-2}$	$0·014 \times 10^{-2}$	0·1
122·1	$0·011 \times 10^{-2}$	$0·011 \times 10^{-2}$	−0·4

The next set of analyses involved a more realistic head model. These studies emphasised the effects of cortical neural source location and orientation in a irregularly shaped head, including the eye orbit region of the skull. The half-head, symmetric to the middle saggital plane, was studied. Approximate geometric data were obtained from a human skull by manual measurement; the thickness of the skull and scalp layer were roughly 4 mm and 5 mm, respectively, but varied at different locations (±1 mm). As in the three-spheres model, a brain or scalp to skull conductivity ratio of 80 was assumed. Also, a similar grid density to that of the three-concentric-spheres model was used, i.e. a total of 8487 nodes and 1834 elements in the half-head model.

Dipoles both perpendicular and parallel to the outer scalp surface were placed at different locations in the symmetric plane, as shown in Fig. 4. They were located at the top of the cortical layer (3 mm below the skull/brain boundary). Finite-element analyses were carried out for each dipole, and the results are shown in Fig. 5. A total of 221 nodes over the scalp surface was used to find an equivalent spherical surface by means of the least-squares fit:

$$Q = \frac{1}{N}\sum_{i=1}^{N}[(x_i - x_m)^2 + (y_i - y_m)^2 + (z_i - z_m)^2 - R^2]$$

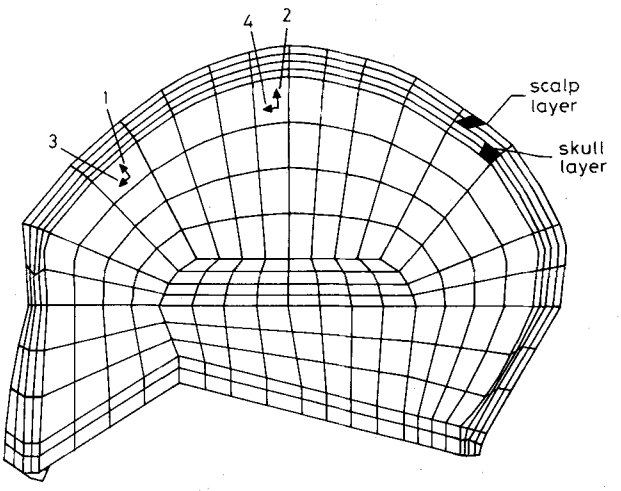

Fig. 4 *Mid-sagittal section of the finite-element model of the head. Label numbers 1–4 indicate four analyses using four different dipoles. The scalp and skull each consist of two layers*

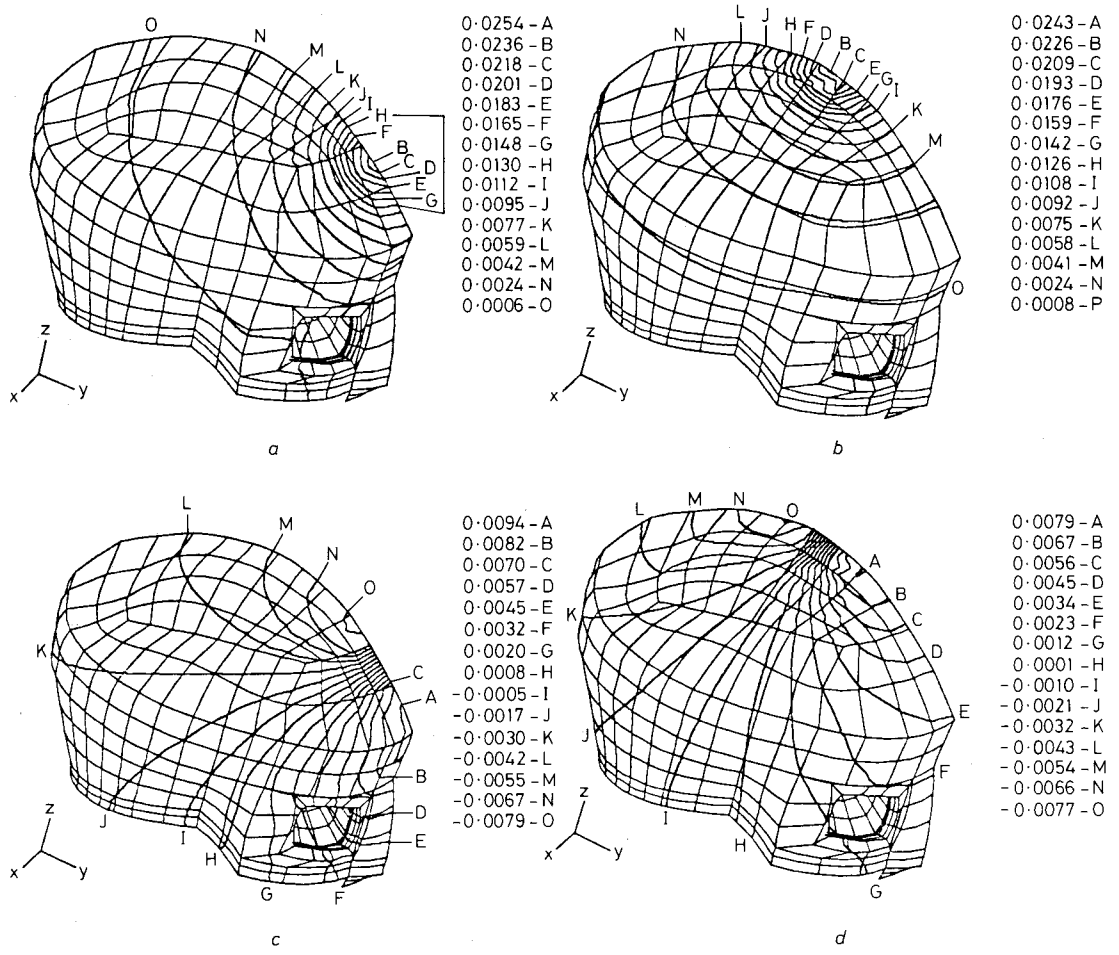

Fig. 5 *Results of finite-element calculations for the four dipoles indicated in Fig. 4*

where (x_i, y_i, z_i) are the co-ordinates of the ith surface location, (x_m, y_m, z_m) are the co-ordinates of the estimated spherical centre and R is the estimated radius of the scalp. Because of the symmetry of the model, x_m is set to 0. The radii of the spheres representing the skull and brain are thus $(R - R_c)$ and $(R - R_c - R_s)$, where R_c and R_s are the thicknesses of the scalp and skull, respectively. The result of this fit is a radius 7·62 cm for the outer surface with a standard deviation of 1·13 cm; the radii of skull and brain tissue are 7·12 cm and 6·72 cm, respectively. It should be noted that these data were obtained from a commercially available skull (probably from India), which was significantly smaller than those expected for Western, adult EEG studies.

Analytic solutions of the three-concentric-spheres model at 221 node positions on the scalp surface were calculated and compared with the results of the finite-element analysis for each dipole case (location and orientation). Differences between the finite-element solutions and analytical solutions in the equivalent layered sphere range from about 10 per cent to about 30 per cent. Also of interest is the question of how surface potential decays as a function of surface distance from the dipole. For the human head model, different decay relationships occur along different directions; only the decay relationship along the middle saggital directions is presented in Fig. 6. Both the finite-element solutions and analytical solutions along this direction are normalised with respect to their respective peak values so that the normalised difference of decay can be observed more clearly.

The effects of the eye orbital structure on scalp surface potential were also studied here. The finite-element simulation of this structure consisted of two layers of elements: one layer representing the bone tissue is 1·0 mm thick on average; this layer merges into the scalp layer, as shown in Fig. 7. Finite-element analyses with dipoles at two different locations were carried out using this model. It should be noted here that these dipoles were not placed in the symmetric plane so that the midline boundary condition is no longer satisfied. However, in a separate study it was shown that the midline boundary condition can be considered approximately satisfied as a result of the dipoles being located relatively far away (3 cm) from the midline in these simulations (YAN, 1988). Examples of two versions of the finite-element analyses involving eye orbits are shown in Fig. 7. In case 1, in which the dipole is placed at the top of the brain tissue, a similar potential distribution to those resulting from cortical dipoles in the middle saggital plane is observed; however, near the orbital region, the potential is small and widely smeared. In case 2, in which the dipole is placed right behind the 'rear wall' of the orbit, a widely smeared and slowly decaying potential is found on the upper scalp region, while near the orbital region a relatively faster decaying potential is observed.

3 Discussion

A three-dimensional finite-element model of the human head based on a new method to characterise dipole sources is presented in this paper. The accuracies of the results were estimated by comparing surface potentials from a finite-element analysis of the three-concentric-spheres model with equivalent analytical solutions. From this comparison it was concluded that the finite-element results using this grid density are quite accurate, and the same general level of accuracy is expected with the realistic head model using a similar grid density.

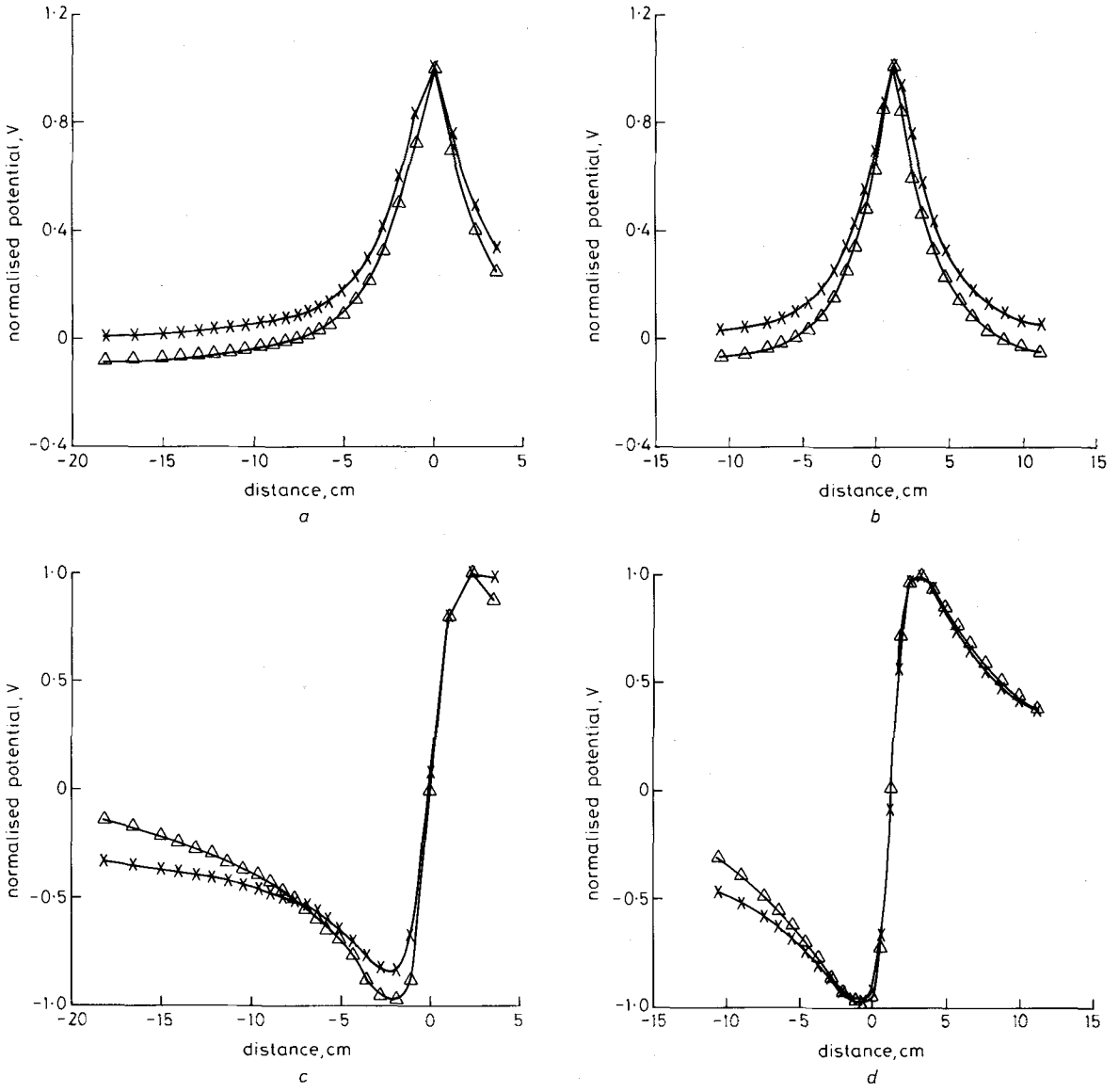

Fig. 6 *Comparisons of the decay relationship between the finite-element analyses and the three-concentric-spheres model analytic solution for scalp potentials at locations along the mid-sagittal direction. (a)–(d) are four comparisons from the four analyses shown in Fig. 5. The x-axis is measured along the surface (cm). The origin of the x-axis is above the dipole. Frontal regions correspond to positive*

The finite-element results are less accurate, although still within an acceptable level for most applications, in regions near the dipole source(s). This inaccuracy occurs because dipoles are modelled as several point sources by performing the mathematical operation presented in the Appendix of this paper. In other words, the equivalent current source is a set of discrete samples of the true and continuous current source. The accuracy of this sampling operation is dependent on the size of the element containing the dipole source. Although satisfactorily accurate for the purpose of analysing surface potential (even when the dipole is placed near the top of the cortex), a denser grid might be required if the potential very close to the source region is of particular interest.

The comparison between the results of the finite-element analyses of the head model and those calculated by the 'equivalent' three-concentric-spheres model shows substantial differences. As both the head and concentric spheres models used here are relatively simple volume conductor models, the resulting potential differences are due only to geometric differences. However, the finite-element model yields approximate estimates of error magnitudes and possible methods for correcting spherical models. It is also noted that in these simulations, the orbital structures contribute relatively minor errors to scalp potentials in the regions where EEG electrodes are normally placed. However, further study using more detailed considerations of geometry and conductivity is required before general conclusions can be obtained about the effects of eye orbits.

The most important attraction of the three-dimensional finite-element analysis which neither spherical models nor two-dimensional finite-element analysis can match is the capability of direct modelling of the detailed structure of the human head. Earlier models, as well as the results presented in this paper, are based on the assumption of isotropic electrical conductivity with the head. However, a number of studies of white matter, cortex and other brain tissue have shown significant anisotropic behaviour (NUNEZ, 1981). Theoretically, the finite-element formulation developed here has the capability to cope with an anisotropic conductive medium; thus, it is possible to develop and analyse more complicated models. A good strategy is probably to add one interesting feature at a time into the model and study its effects. These kinds of future parameter studies will be mostly limited by methods to accurately estimate electrical conductivities of different tissues in the living human head. Such estimates may, in theory, be obtained from simultaneous knowledge of both

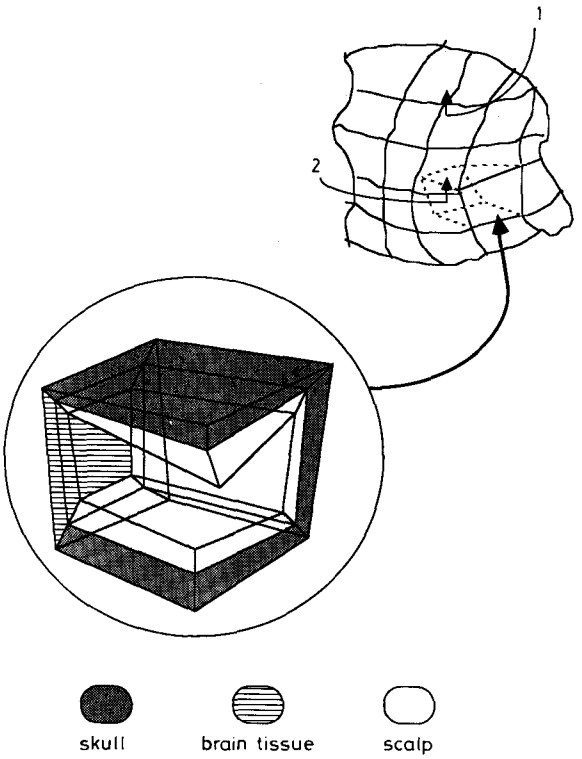

Fig. 7 *Studies of the eye orbit structure are summarised here. An illustration of the orbit structure in the finite-element model is shown. Numbers 1 and 2 represent two analyses using a dipole located as indicated. Both dipoles are located 3 cm off the symmetric plane and are oriented vertically as shown*

sources and surface potentials so that classical boundary value problems are overspecified (NUNEZ, 1987*b*).

Acknowledgment—This research was partly supported by US National Institutes of Health grant 1R01N524314.

References

ARY, J. P., KLEIN, S. A. and FENDER, D. H. (1981) Location of sources of evoked scalp potentials: corrections for skull and scalp thickness. *IEEE Trans.*, **BME-28,** 447–452.

COOK, R. (1981) *Concepts and applications of finite element analysis.* Wiley, New York.

DHATT, G. and TOUZOT, G. (1984) *The finite element method displayed.* Wiley, New York.

HE, B. BUSHA, T., OKAMOTO, Y., HOMMA, S., NAKAJIMA, Y. and SATO, T. (1987) Electric dipole tracing in the brain by means of the boundary element method and its accuracy. *IEEE Trans.*, **BME-34,** 406–413.

HINTON, E. and OWEN, D. (1984) *Finite element software for plates and shells.* Pineridge Press.

HUEBNER, K. and THORNTON, E. (1984) *The finite element method for engineers.* Wiley, New York.

MEIJS, J. and PETERS, M. (1987) The EEG and EMG, using a model of eccentric spheres to describe the head. *IEEE Trans.*, **BME-34,** 913–920.

NUNEZ, P. (1981) *Electric fields of the brain: the neurophysics of EEG.* Oxford University Press, New York.

NUNEZ, P. L. (1987*a*) Removal of reference electrode and volume conduction effects by spatial deconvolution of evoked potentials using a three-concentric sphere model of the head. The London Symposium. *Electroencephal. Clin. Neurophysiol.*, **39,** Suppl., 143–148.

NUNEZ, P. L. (1987*b*) A method to estimate local skull resistance in living subjects. *IEEE Trans.*, **BME-34,** 902–904.

NUNEZ, P. L. (1989) Estimation of large scale neocortical source activity with EEG surface Laplacians. *Brain Topography*, **2,** 141–154.

NUNEZ, P. L. (1990) Localization of brain activity with electroencephalography. In *Advances in neurology, Vol. 54 Magnetoencephalography*, SATO, S. (Ed.), Raven Press, 39–65.

PLONSEY, R. (1969) *Bioelectric phenomena.* McGraw-Hill, New York.

RUSH, S. and DRISCOLL, D. (1968) Current distribution in the brain from surface electrodes. *Anesth. & Analg.*, **47,** 717–723.

RUSH, S. and DRISCOLL, D. (1969) EEG electrode sensitivity: an application of reciprocity. *IEEE Trans.*, **BME-16,** 15–22.

SCHERG, M. and VON CRAMON, D. (1985) Two bilateral sources of the late AEP as identified by spatio-temporal dipole model. *Electroenceph. Clin. Neurophysiol.*, **62,** 32–44.

SEPULVEDA, N., WALKER, C. and HEATH, R. (1983) Finite element analysis of current pathways with implanted electrodes. *J. Biomed. Eng.*, **5,** 41–48.

SEPULVEDA, N. (1984) Electric field distribution in three dimensional regions using the finite element method. Ph.D. Dissertation, Tulane University, New Orleans, Louisiana, USA.

YAN, Y. (1988) A finite element model of the human head—surface potentials due to dipole sources in the brain. MS Thesis, Tulane University, New Orleans, Louisiana, USA.

Appendix

The electric potential $v(x, y, z)$ that results from a current source $I(x, y, z)$ in a volume conductor is described by the semiharmonic field equation:

$$\nabla \cdot (k\nabla v) + I = 0 \quad \text{on } \Omega \tag{1}$$

defined over a spatial domain Ω, and governed by boundary conditions

$$v = U(x, y, z) \quad \text{on } S_1 \tag{2}$$

$$k\nabla v \cdot n = g(x, y, z) \quad \text{on } S_2 \tag{3}$$

The non-overlapping surfaces S_1 and S_2 compose a closed boundary surface of Ω, as shown in Fig. 1.

The method of Galerkin's weighted residuals is used here to solve the above equations (COOK, 1981; HUEBNER and THORNTON, 1984; DHATT and TOUZOT, 1984). An approximate solution $v(x, y, z)$ is assumed which satisfies

$$\iiint_{\Omega} \left[\frac{\partial}{\partial x}\left(k_x \frac{\partial v}{\partial x}\right) + \frac{\partial}{\partial y}\left(k_y \frac{\partial v}{\partial y}\right) + \frac{\partial}{\partial z}\left(k_z \frac{\partial v}{\partial z}\right) + I \right] W \, d\Omega = 0 \tag{4}$$

where W is called the weighting function. Integration of eqn. 4 by parts yields

$$\iint_{S_2} \left[n_x \frac{\partial v}{\partial x} k_x + n_y \frac{\partial v}{\partial y} k_y + n_z \frac{\partial v}{\partial z} k_z \right] W \, dS_2 - \iiint_{\Omega} \left[k_x \frac{\partial v}{\partial x}\frac{\partial W}{\partial x} + k_y \frac{\partial v}{\partial y}\frac{\partial W}{\partial y} + k_z \frac{\partial v}{\partial z}\frac{\partial W}{\partial z} + IW \right] d\Omega = 0 \tag{5}$$

Combine eqns. 3 and eqns 5, and reorganise to obtain

$$\iiint_{\Omega} \left[k_x \frac{\partial v}{\partial x}\frac{\partial W}{\partial x} + k_y \frac{\partial v}{\partial y}\frac{\partial W}{\partial y} + k_z \frac{\partial v}{\partial z}\frac{\partial W}{\partial z} \right] d\Omega = \iiint_{\Omega} IW \, d\Omega - \iint_{S_2} gW \, dS_2 \tag{6}$$

Now consider v, which is expressed as

$$v \approx V = \sum_{i=1}^{m} N_i C_i \tag{7}$$

The N_is comprise the assumed shape function, and C_is are unknown coefficients to be solved for. According to the Galerkin method, the weighting function Ws are chosen such that

$W_i = N_i$. Then, eqns. 6 and 7 combine to yield

$$\sum_{j=1}^{m} C_j \iiint_{\Omega} \left(k_x \frac{\partial N_j}{\partial x}\frac{\partial N_i}{\partial x} + k_y \frac{\partial N_j}{\partial y}\frac{\partial N_i}{\partial y} + k_z \frac{\partial N_j}{\partial z}\frac{\partial N_i}{\partial z} \right) d\Omega = \iiint_{\Omega} I\, N_i\, d\Omega - \iint_{S_2} g N_i\, dS_2 \quad i = 1, 2, \ldots, m \quad (8)$$

Eqn. 8 is a system containing m linear equations and m unknowns, i.e. the m C_is.

In the finite-element analysis, the whole solution domain Ω is divided into a set of subdomains (element domains) $\Omega_i^{(e)}$s. We apply the above methods to each element domain, and nodal values are set as the unknown coefficients so as to obtain

$$\sum_{j=1}^{m} V_j \iiint_{\Omega^{(e)}} \left(k_x \frac{\partial N_j^{(e)}}{\partial x}\frac{\partial N_i^{(e)}}{\partial x} + k_y \frac{\partial N_j^{(e)}}{\partial y}\frac{\partial N_i^{(e)}}{\partial y} + k_z \frac{\partial N_j^{(e)}}{\partial z}\frac{\partial N_i^{(e)}}{\partial z} \right) d\Omega^{(e)} = \iiint_{\Omega^{(e)}} I\, N_i^{(e)}\, d\Omega^{(e)} - \iint_{S_2^{(e)}} g N_i^{(e)}\, dS_2^{(e)} \quad (9)$$

or, in the matrix form

$$[\boldsymbol{K}]^{(e)}\{\boldsymbol{V}\}^{(e)} = \{\boldsymbol{F}\}^{(e)} \quad (10)$$

in which

$$k_{ij} = \iiint_{\Omega^{(e)}} \left(k_x \frac{\partial N_j^{(e)}}{\partial x}\frac{\partial N_i^{(e)}}{\partial x} + k_y \frac{\partial N_j^{(e)}}{\partial y}\frac{\partial N_i^{(e)}}{\partial y} + k_z \frac{\partial N_j^{(e)}}{\partial z}\frac{\partial N_i^{(e)}}{\partial z} \right) d\Omega^{(e)} \quad (11)$$

$$f_i = \iiint_{\Omega^{(e)}} I\, N_i^{(e)}\, d\Omega^{(e)} - \iint_{S_2^{(e)}} g N_i^{(e)}\, dS_2^{(e)} \quad (12)$$

These element equations are assembled into a global equation system, and the solution to the global system is the nodal values of V.

An ideal current dipole is described as two point sources of opposite polarity with infinitely large current density and an infinitely small separation, i.e.

$$I(\boldsymbol{r}) = I_0 \left[\delta\left(\boldsymbol{r} - \boldsymbol{r}_0 - \frac{\boldsymbol{d}}{2}\right) - \delta\left(\boldsymbol{r} - \boldsymbol{r}_0 + \frac{\boldsymbol{d}}{2}\right) \right] \quad (13)$$

Substitute this expression into eqn. 10 to obtain

$$\iiint_{\Omega^{(e)}} I\, N_i^{(e)}\, d\Omega^{(e)} = \lim_{d \to 0} I_0 \left[N_i^{(e)}\left(\boldsymbol{r}_0 + \frac{\boldsymbol{d}}{2}\right) - N_i^{(e)}\left(\boldsymbol{r}_0 - \frac{\boldsymbol{d}}{2}\right) \right] = I_0\, \boldsymbol{d} \cdot \nabla N_i^{(e)}(\boldsymbol{r}_0) \quad (14)$$

Through this operation the mathematical dipole is replaced by a number of point sources, i.e. one point source for each node of the element. The accuracy of this operation still depends on the size of the element because the shape functions are only an approximation of the true field (HINTON and OWEN, 1984); however, numerical results presented in this paper show that satisfactory accuracy is achieved by selecting a suitable grid density. Because dipoles can be located anywhere within an element in this formulation, the size of the element need not match the small pole separation of the dipole. If dipole locations and/or orientation are changed, the finite-element model does not require modification. The advantage of this formulation is more obvious if many dipoles are included in the same simulation. For example, many EEG phenomena are believed to be due to large, neocortical dipole layers which may require hundreds or thousands of single dipoles in the appropriate simulation (NUNEZ, 1981; 1989; 1990).

The numerical solutions obtained here were compared to the analytical solution for the surface potential in a three-concentric-spheres model; i.e. the electrical potential at the outmost surface resulting from a single radial dipole located at a radius r_0 (within the inner sphere) may be expressed as the following sum over Legendre polynomials P (NUNEZ, 1981; RUSH and DRISCOLL, 1968).

$$v(\theta) = \frac{Id}{2\pi k_3 c^2} \sum_{l=1}^{\infty} A_l l \left(\frac{r_0}{c}\right)^{l-1} P_l(\cos\theta) \quad (15)$$

where the series coefficients are given by

$$A = [(2l+1)^3/2l]\{[(k_1/k_2 + 1)l + 1][(k_2/k_3 + 1)l + 1] + l(l+1)(k_1/k_2 - 1)(k_2/k_3 - 1)(a/b)^{2l+1} + (l+1)(k_2/k_3 - 1)[(k_1/k_2 + 1)l + 1](b/c)^{2l+1} + (l+1)(k_1/k_2 - 1)[(k_2/k_3 + 1)(l+1) - 1](a/c)^{2l+1}\}^{-1} \quad (16)$$

Here a, b and c are the radii of the inner, middle and outer spherical surfaces, respectively. Also, k_1, k_2 and k_3 are electrical conductivities of these regions. θ is the angle between the dipole and the radial vector locating the surface field point. In the case of a non-radial dipole, eqn. 15 requires modification. The more general solution is given in ARY *et al.* (1981).

Authors' biographies

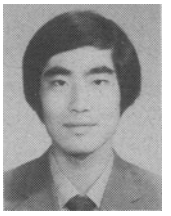

Yuchen Yan was born in Shanghai, People's Republic of China, in 1964. He received his B.Sc. degree in Biomedical Engineering from Shanghai Jiao Tong University, Shanghai, China, in 1986 and his M.Sc. degree in Biomedical Engineering from Tulane University, New Orleans, Louisiana, USA, in 1988. He is a research associated in the School of Medicine, George Washington University, Washington, DC and the National Institutes of Health, Bethesda, Maryland. His interests are in positron emission tomographic instrumentation and application, in kinetic modelling and other algorithm research.

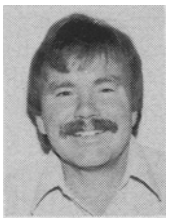

Paul L. Nunez was born in Miami Beach, Florida, USA, in 1940. He received BS, and MS degrees in Aerospace Engineering from the University of Florida in 1962 and 63, respectively, and a Ph.D. in Engineering Science from the University of California at San Diego in 1969. He has studied the neurosciences, worked in both industry and academia on spaceflight, fusion and neuroscience, and is currently Professor of Biomedical Engineering at Tulane University, New Orleans, Louisiana. His scientific interests encompass theoretical and experimental aspects of electroencephalography, including nonlinear phenomena, signal processing, cognitive studies and medical applications.

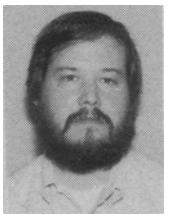

Richard T. Hart received a Bachelor of Engineering Science in 1975, and an MS in Engineering Mechanics in 1977, both from the Georgia Institute of Technology in Atlanta, Georgia, USA. He received a scholarship to study for a year at the Technische Universität Berlin, West Germany, 1977–1978. He received his Ph.D. degree in 1983 from the Department of Mechanical & Aerospace Engineering, Case Western Reserve University, Cleveland, Ohio. He is currently an Associate Professor in the Department of Biomedical Engineering at Tulane University, New Orleans, Louisiana. He is a member of a number of technical and scientific societies.